Supplementary Information:

in situ surface-enhanced electronic and vibrational Raman scattering spectroscopy at metal/molecule interfaces

Motoharu Inagaki,[1] *Kenta Motobayashi,* [1] *and Katsuyoshi Ikeda**[,1,2]

[1] Department of Physical Science and Engineering, Nagoya Institute of Technology, Gokiso, Showa, Nagoya 466-8555, Japan.

[2] Frontier Research Institute for Materials Science (FRIMS), Nagoya Institute of Technology, Gokiso, Showa, Nagoya 466-8555, Japan.

*Corresponding Authors: kikeda@nitech.ac.jp

.

1. Correction of normal Raman and surface-enhanced Raman spectra

The calculation method to reduce various factors from measured normal Raman and SERS spectra is briefly summarized here. For more details, see Ref. 21 and references therein. The power spectrum of vibrational Raman scattering (VRS) in the absence of plasmonic enhancement, $I_{\mathrm{RS}}(\nu^{\Delta})$, is expressed by:

$$I_{\mathrm{RS}}(\tilde{\nu}_{\mathrm{s}}^{\Delta}) = K(\tilde{\nu}_{\mathrm{i}} - \tilde{\nu}_m)^3[n(\tilde{\nu}_m) + 1]\chi''_{\mathrm{VRS}}(\tilde{\nu}_m) \quad \text{(S1)}$$

for the Stokes branch and

$$I_{\mathrm{RS}}(\tilde{\nu}_{\mathrm{as}}^{\Delta}) = K(\tilde{\nu}_{\mathrm{i}} + \tilde{\nu}_m)^3[n(\tilde{\nu}_m) \quad]\chi''_{\mathrm{VRS}}(\tilde{\nu}_m) \quad \text{(S2)}$$

for the anti-Stokes branches. Here, $\tilde{\nu}_{\mathrm{i}}$ and $\tilde{\nu}_{\mathrm{m}}$ are the photon energy for the incident laser in cm^{-1} and the molecular vibration energy in cm^{-1}, respectively. $\tilde{\nu}_{\mathrm{s}}^{\Delta}$ and $\tilde{\nu}_{\mathrm{as}}^{\Delta}$ are the Raman shifts in the Stokes and anti-Stokes branches, *i.e.*, $\tilde{\nu}_{\mathrm{s}}^{\Delta} = \tilde{\nu}_m$ and $\tilde{\nu}_{\mathrm{as}}^{\Delta} = -\tilde{\nu}_m$. $\chi''_{\mathrm{VRS}}(\tilde{\nu}_m)$ is the imaginary part of the dynamical susceptibility for VRS. The cubic terms of the scattering photon energies, $(\tilde{\nu}_{\mathrm{i}} - \tilde{\nu}_m)^3$ and $(\tilde{\nu}_{\mathrm{i}} + \tilde{\nu}_m)^3$, express the scattering efficiency factors for the Stokes and anti-Stokes branches when when $I_{\mathrm{RS}}(\nu^{\Delta})$ is measured by photon counting method. $n(\tilde{\nu}_m)$ is the Bose-Einstein distribution described as $n(\tilde{\nu}_m) = [\exp(hc\tilde{\nu}_m/k_{\mathrm{B}}T) - 1]^{-1}$, where h, c, k_{B} and T are Planck's constant, the velocity of light, the Boltzmann constant, and local temperature, respectively. K is an instrument constant.

The power spectrum of electronic Raman scattering (ERS) in the absence of plasmonic enhancement is expressed in a similar manner; $\chi''_{\mathrm{VRS}}(\tilde{\nu}_m)$ in Eqns. (S1) and (S2) is replaced with $\chi''_{\mathrm{ERS}}(\tilde{\nu}_m)$, which is determined by integrating the thermally occupied electronic states over the distribution of excited wave vectors. Apparently, $\chi''_{\mathrm{ERS}}(\tilde{\nu}_m)$ depends on the excitation energy and local temperature, which is different from the nature of $\chi''_{\mathrm{VRS}}(\tilde{\nu}_m)$. It is here emphasized that the thermal

factor connecting the power spectrum and the susceptibility should be described by the Bose-Einstein function while the $\chi''_{\mathrm{VRS}}(\tilde{\nu}_m)$ is related to the Fermi-Dirac function.

In the presence of plasmonic enhancement, the connection between the power spectrum and the susceptibilities must include the local field enhancement effect for both incoming and outgoing lights in addition to the Bose-Einstein thermal factor and the scattering efficiency factor. Thus, the power spectrum of SERS, $I_{\mathrm{SERS}}(\nu^{\Delta})$, is expressed by:

$$I_{\mathrm{SERS}}(\tilde{\nu}_{\mathrm{s}}^{\Delta}) = K(\tilde{\nu}_{\mathrm{i}} - \tilde{\nu}_m)^3[n(\tilde{\nu}_m) + 1]$$
$$\times \left([f_{\mathrm{VSERS}}(\tilde{\nu}_{\mathrm{i}} - \tilde{\nu}_m)]^2[f_{\mathrm{VSERS}}(\tilde{\nu}_{\mathrm{i}})]^2 g_{\mathrm{V}}\chi''_{\mathrm{VRS}}(\tilde{\nu}_m) + [f_{\mathrm{ESERS}}(\tilde{\nu}_{\mathrm{i}} - \tilde{\nu}_m)]^2[f_{\mathrm{ESERS}}(\tilde{\nu}_{\mathrm{i}})]^2 g_{\mathrm{E}}\chi''_{\mathrm{ERS}}(\tilde{\nu}_m)\right) \quad \text{(S3)}$$

for the Stokes branch and

$$I_{\mathrm{SERS}}(\tilde{\nu}_{\mathrm{as}}^{\Delta}) = K(\tilde{\nu}_{\mathrm{i}} + \tilde{\nu}_m)^3[n(\tilde{\nu}_m) \quad]$$
$$\times \left([f_{\mathrm{VSERS}}(\tilde{\nu}_{\mathrm{i}} + \tilde{\nu}_m)]^2[f_{\mathrm{VSERS}}(\tilde{\nu}_{\mathrm{i}})]^2 g_{\mathrm{V}}\chi''_{\mathrm{VRS}}(\tilde{\nu}_m) + [f_{\mathrm{ESERS}}(\tilde{\nu}_{\mathrm{i}} + \tilde{\nu}_m)]^2[f_{\mathrm{ESERS}}(\tilde{\nu}_{\mathrm{i}})]^2 g_{\mathrm{E}}\chi''_{\mathrm{ERS}}(\tilde{\nu}_m)\right) \quad \text{(S4)}$$

for the anti-Stokes branch. Here, f denotes the local field enhancement: $f \equiv \left|E_{\text{near-field}}/E_{\text{far-field}}\right|$ and g is the coupling efficiency of electronic or vibrational Raman transitions to the plasmonic nano-cavity. $[f_{\mathrm{ESERS}}(\tilde{\nu}_{\mathrm{i}} \pm \tilde{\nu}_m)]^2$ and $[f_{\mathrm{VSERS}}(\tilde{\nu}_{\mathrm{i}} \pm \tilde{\nu}_m)]^2$ correspond to the Purcell factor. Here, one can obtain $\chi''_{\mathrm{ERS}}(\tilde{\nu}_m)$ by measuring normal ERS spectrum of a smooth Au surface. Therefore, when the SERS background continuum is purely originated from plasmonic enhancement of ERS, one can estimate the term of $[f_{\mathrm{ESERS}}(\tilde{\nu}_{\mathrm{i}} + \tilde{\nu}_m)]^2[f_{\mathrm{ESERS}}(\tilde{\nu}_{\mathrm{i}})]^2 g_{\mathrm{E}}$, including the Purcell factor, from the comparison between SERS spectrum of a roughened Au surface and ERS spectrum of a smooth Au. By assuming that the ratio of the local field enhancement on both sides of the metal/dielectric interface is constant, the susceptibilities for VRS and ERS can be extracted from measured SERS spectra.

2. Measured and calculated spectra of normal Raman and SERS

Figure S1(a) shows the normal VRS spectrum for MBT molecules in a liquid state, measured at 320 K. When this spectrum is corrected using Eqns. (s1) and (s2), the Stokes and anti-Stokes branches becomes symmetric as shown in Fig. S1(b), indicating that the Bose-Einstein thermal factor and the scattering efficiency factor are properly reduced from the measured spectrum. There is a broad feature below 200 cm^{-1} in addition to distinctive Raman bands of a MBT molecule. Given that such a broad feature is often observed in various solutions such as ionic liquids, this is probably related to collective motions of MBT molecules interacting neighboring molecules in liquid state. On the other hand, as reported in Ref. 21, the crystalline MBT molecules exhibit more distinctive Raman band in this region. Since the crystallinity of MBT-SAMs is much lower than that in solid state, both the liquid-like broad feature and the crystalline peak of δAuS-Ph presumably appeared in SERS spectra for MBT-SAMs.

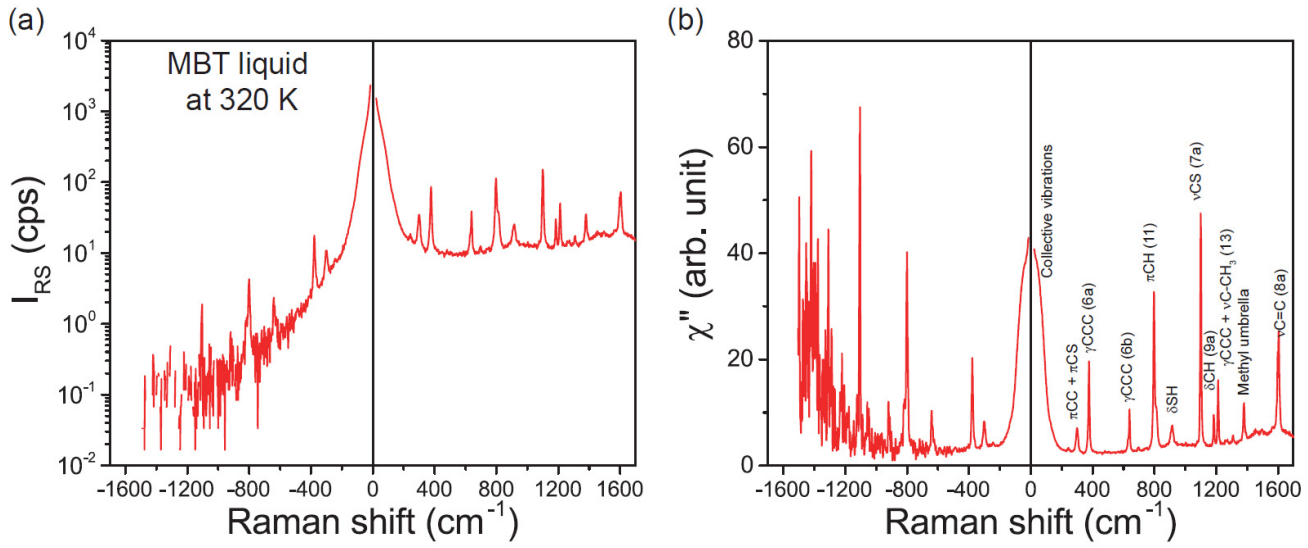

Fig. S1. (a) Normal VRS power spectrum for MBT molecules in a liquid state measured at 320 K. (b) VRS susceptibility spectrum for MBT, obtained by reducing the Bose-Einstein thermal factor and the scattering efficiency factor from (a).

Figure S2 shows SERS spectra for Au/MBT-SAMs under the positive-going potential scan in 0.1 M KOH solution, corrected for the Purcell factor, the Bose-Einstein thermal factor, and the scattering efficiency factor, based on Eqns. (S3) and (S4). It is clear that both the VRS peaks and the ERS continuum are nearly symmetric for the Stokes and anti-Stokes branches (at least in the lower Raman-shift region below 1000 cm^{-1}). This means that the Purcell factor can be properly reduced from measured SERS spectra as well as the other factors. That is, the origin of the background continuum can be indeed ascribed to ERS. While the Stokes and anti-Stokes branches provide identical information, the reliability of the calculation results can be examined by comparing both branches.

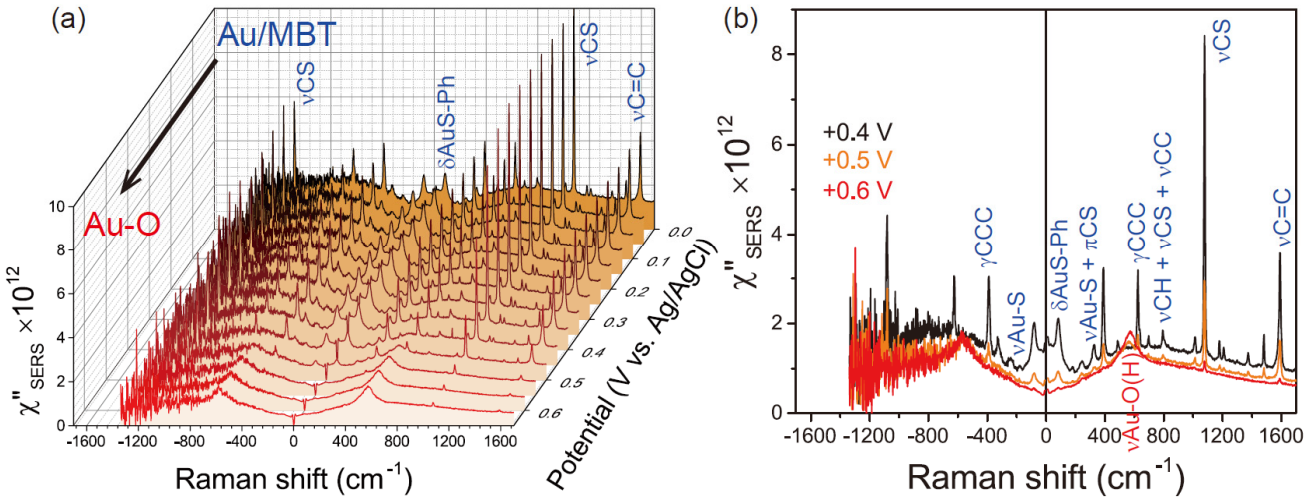

Fig. S2. (a) A series of SERS spectra for Au/MBT-SAMs under the positive-going potential scan in 0.1 M KOH solution. (b) SERS spectra taken at +0.4, +0.5 and +0.6 V vs. Ag/AgCl. All spectra are corrected for the Bose-Einstein thermal factor, the Purcell factor, and the scattering efficiency factor.

Figure S3 shows SERS spectra for Au/MBT-SAMs under the negative-going potential scan in 0.1 M KOH solution, corrected for the Purcell factor, the Bose-Einstein thermal factor, and the scattering efficiency factor. Again, the spectral features of the VRS peaks and the ERS continuum are symmetric between the Stokes and anti-Stokes branches, indicating that the susceptibilities are properly

extracted from the measured spectra. In the low-frequency region, enlarged in Fig. S3(c), the Au-S related vibrations such as νAu-S, νAu-S + πCS, and γCCC are red shifted at −1.0 V compared with those at −0.5 V, as a result of the weakened Au-S bond strength.

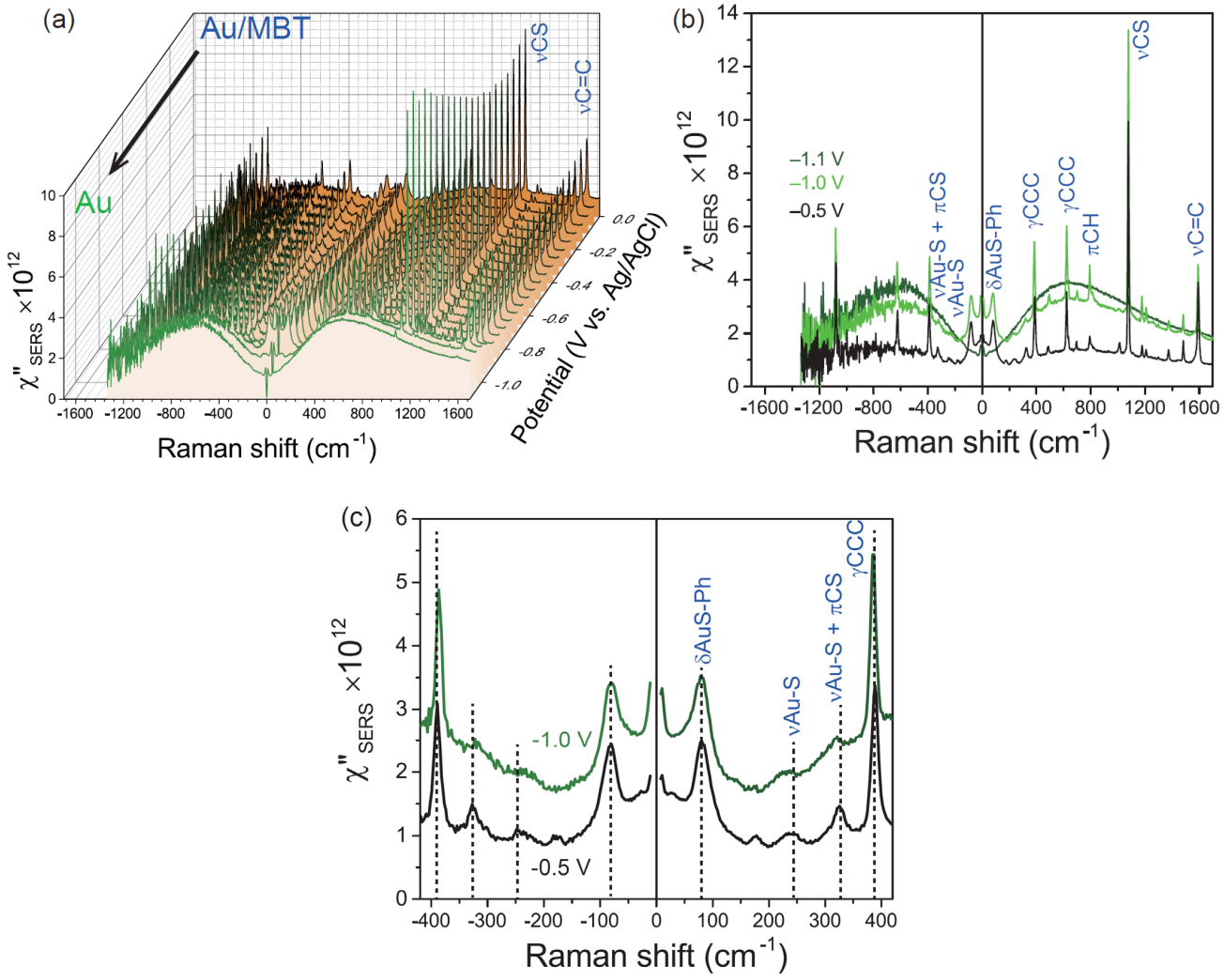

Fig. S3. (a) A series of SERS spectra for Au/MBT-SAMs under the negative-going potential scan in 0.1 M KOH solution. (b) SERS spectra taken at −0.5, −1.0 and −1.1 V vs. Ag/AgCl. (c) Enlarged low-frequency region of the SERS spectra at −0.5 and −1.0 V vs. Ag/AgCl. All spectra are corrected for the Bose-Einstein thermal factor, the Purcell factor, and the scattering efficiency factor.

3. Cyclic voltammogram for Au/MBT-SAMs

Figure S4(a) shows first and second cycles of the cyclic voltammogram for Au/MBT-SAM in 0.1 M KOH solution. An oxidative broad peak in the range of 0.4 – 0.8 V is ascribed to the growth of surface oxide layers, which is positively shifted from the peak found at 0.3 V in the second cycle. This indicates that the surface oxide formation is hindered by the presence of MBT-SAMs on the surface. The anodic current due to the oxygen evolution and the reductive peak of the surface oxides at 0.11 V are almost same for the first and second cycles. Therefore, MBT-SAMs were completely removed from the surface during the first potential scan. This can be confirmed by measuring CVs for bare Au surface, as shown in Fig. S4(b).

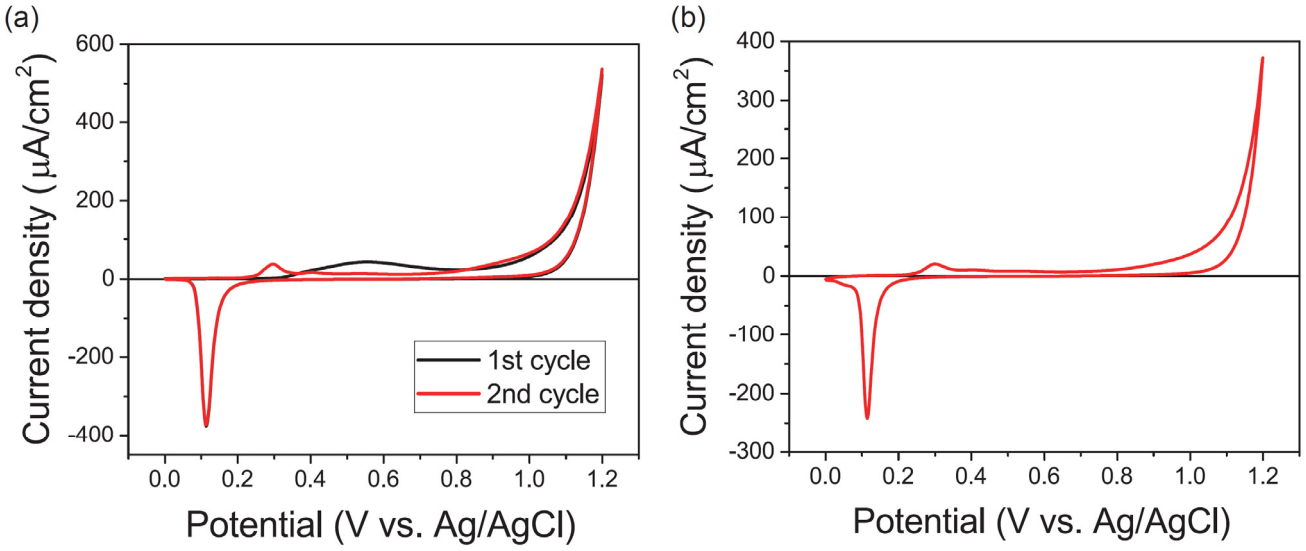

Fig. S4. (a) Cyclic voltammogram for roughened Au/MBT-SAM in 0.1 M KOH solution. The current density was calculated for the surface area before application of the surface roughening. (b) Cyclic voltammogram for bare Au without surface roughening in 0.1 M KOH solution. Both voltammograms were obtained with the scan rate of 20 mV/s.

4. Formation of MBT-SAMs on Au surface

Figure S5 shows *in situ* SERS observation of the formation of MBT-SAMs on Au surface in ethanol. The intensity change of the broad feature below 200 cm^{-1} was determined using the intensity difference between 26 cm^{-1} and 146 cm^{-1}, which corresponds to the baseline for δAuS-Ph, because it was difficult to perform deconvolution from the ERS background.

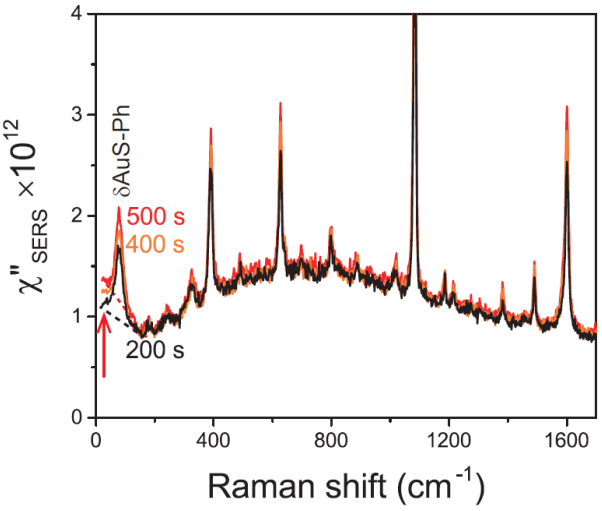

Fig. S5. Corrected SERS spectra for the bare Au surface in ethanol, taken at 200, 400, and 500 s after MBT molecules were injected to the cell.

5. Vibration modes of the model molecule

Table S1 summarizes calculated and measured vibration modes of MBT with and without Au-S bonding. Vibration modes of MBT were calculated using the GAUSSIAN 09 revision A02 at the B3LYP level of theory with LanL2DZ basis set for Au atom and 6-31G** basis sets for other atoms. Experimental values for normal Raman and SERS spectra were taken from Fig. S1(b) and Fig. 3, respectively. The

assignment of δAuS-Ph in SERS was based on the peak shift between benzethiol derivatives, as reported in Ref. 25.

Table S1. Calculated and measured frequencies (cm^{-1}) of Raman bands of MBT

Isolated (calc.)	Attached to Au (calc.)	Raman (measured)	SERS (measured)	assignments
–	–	–	78	δAuS-Ph (hinge bending of Au-S-phenyl ring)
–	260	–	235	νAu-S
289		300		πCC + πCS
	344		326	(+ νAu-S)
363	366	376	389	γCCC, 6a
627	611	640	623	γCCC, 6b
783	1298	797	794	πCH, 11
899	–	918	–	δSH
1075	1056	1100	1078	νCS, 7a
1171	1162	1184	1179	δCH, 9a
1191	1188	1213	1209	γCCC + νC-CH_3, 13
1372	1370	1380	1374	Methyl umbrella
1596	1582	1605	1593	νCC, 8a